

VORD: Visual Ordinal Calibration for Mitigating Object Hallucinations in Large Vision-Language Models

Dexter Neo, Tsuhan Chen
School of Computing
National University of Singapore

e0534450@u.nus.edu, tsuhan@nus.edu.sg

Abstract

Large Vision-Language Models (LVLMs) have made remarkable developments along with the recent surge of large language models. Despite their advancements, LVLMs have a tendency to generate plausible yet inaccurate or inconsistent information based on the provided source content. This phenomenon, also known as “hallucinations” can have serious downstream implications during the deployment of LVLMs. To address this, we present VORD a simple and effective method that alleviates hallucinations by calibrating token predictions based on ordinal relationships between modified image pairs. VORD is presented in two forms: 1.) a minimalist training-free variant which eliminates implausible tokens from modified image pairs, and 2.) a trainable objective function that penalizes unlikely tokens. Our experiments demonstrate that VORD delivers better calibration and effectively mitigates object hallucinations on a wide-range of LVLM benchmarks. Our code is available at: <https://github.com/dexterdley/VORD>.

1. Introduction

Vital requirements for the large-scale adoption of Large Vision-Language Models (LVLMs) include their correctness and faithfulness of generated content. Although LVLMs have achieved significant success in performing complex tasks such as image captioning [20] and visual question answering [71], they are prone to “hallucinations”. Specifically, LVLMs tend to have **object hallucinations** (OH) - instances where the model produces plausible yet incorrect descriptions that are inconsistent to the given visual context cues.

Hallucinations remain a major obstacle for the deployment of LVLMs in high-stakes, risk-sensitive applications, such as healthcare [62, 68], autonomous agents [5, 24, 43, 63] and legal AI [65, 74], where they can result in unsafe or undesirable outcomes. These downstream tasks require

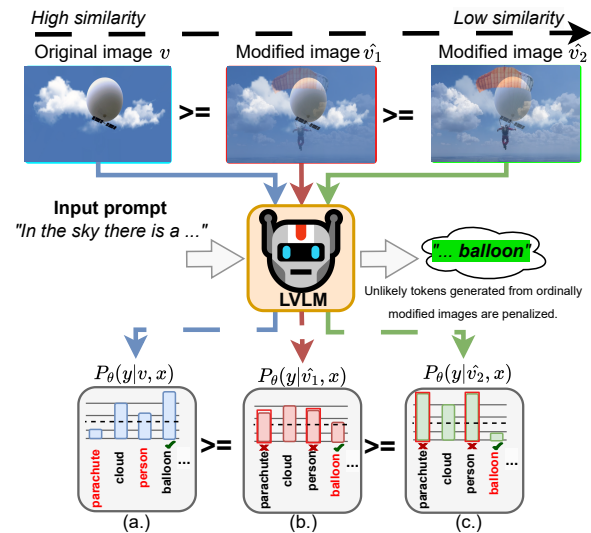


Figure 1. VORD suppresses hallucinated objects such as `<person>` by enforcing ordinal ranking of confidences and penalizing unlikely tokens during the generation process.

LVLMs to not only be accurate but also confident about their predictions. Making it essential for LVLMs to be able to communicate their uncertainty in the event of OH.

The challenge behind mitigating OH comes from the underlying fundamental issues with visual-question answering benchmarks, such as the over-dependence of the natural language priors embedded in the backbone large language model and the prevalent statistical imbalances in the training corpus [11, 26]. Fig. 1 illustrates this phenomenon, where incorrect tokens such as `<person>` and `<parachute>` can have non-zero probabilities, leaving them susceptible to being mistakenly sampled during generation, resulting in object hallucinations.

While numerous efforts have been placed on how to reduce OH in LVLMs [11, 22, 26, 69, 77]. Current studies tend to focus on improving the overall accuracy of LVLMs,

leaving the critical aspect of model confidence calibration in OH largely unaddressed. Since model calibration seeks to align a model’s confidence with its correctness, well-calibrated token generation could also directly lead to better text generations in LVLMs.

Recent works [60] have shown that visual language models such as CLIP [51] are innately better calibrated than other models trained on ImageNet [14, 45]. While other studies [50, 59] have suggested that calibration can be significantly reduced after additional fine-tuning, due to the quality and distribution of the training corpus. Following this line of research, our goal is to reduce object hallucinations, while improving LVLM calibration.

In this paper, we first show that when left unchecked, LVLMs tend to have tokenwise probabilities that do not conform to ranked ordinal relationships when faced with *visually corrupted* inputs (see Sec. 3.4). Building upon this observation, we propose **Visual Ordinal (VORD)** calibration for mitigating object hallucinations in LVLMs. VORD can be implemented as a lightweight, minimalist *training-free* decoding strategy or used as a fully optimizable *objective function* if training resources are available. We demonstrate that VORD effectively mitigates object hallucinations in LVLMs, along with better calibrated predictions and shorter generated text sequences on a wide plethora of object hallucination benchmarks. Our main contributions are summarized as follows:

- **Visually Ordinal Tokens** We demonstrate that when faced with corrupted visual cues, LVLMs do not exhibit well-ordered token probability distributions.
- **VORD Decoding:** We present VORD Decoding, a lightweight, minimalist and training-free method for contrastive decoding in LVLMs.
- **VORD Loss:** We also present VORD Loss, an ordinal ranking loss function for improving performance and mitigating hallucinations in LVLMs.
- **Adaptive Visual Similarity Margin:** Additionally, we enforce the transitive properties of VORD with a novel dynamic visual-similarity penalty margin

2. Related Work

Visual Language Models Given the recent influx of large language models (LLMs), LVLMs have demonstrated incredible capabilities across a multitude of applications. Initial works on VLMs include BERT-based text decoders [9, 40] that integrate textual and visual inputs [27, 28, 56, 61]. Presently, a large focus of LVLM research pivots on Visual Instruction Fine-tuning [31, 36, 37] which extends instruction tuning from NLP research to allow LVLMs to learn on text-image pairs with instructions or descriptions of the image. This process allows backbone LLMs such as LLaMA [58] to better “see” visual tokens and understand the context, delivering better performance on a wide range of tasks

such as image captioning and visual question answering.

Hallucinations in LVLMs Despite their incredible advancements, LVLMs are susceptible to generating plausible-sounding yet ungrounded falsehoods [11]. This phenomena also widely referred to as “hallucinations” [32, 55, 66, 72, 76] have mystified researchers in both the NLP and CV communities [25]. Various approaches have been proposed on how to better reduce OH in LVLMs, all closely related to our work. These include self-correction and self-questioning techniques [57, 69, 77] that ground the LVLM to object/statistical evidence. Other works include training-free decoding approaches that aim to alleviate OH by either reducing/penalizing reliance on textual priors [6, 11, 22, 26]. Parallel to this line of research, our work seeks to better analyze hallucinations from a confidence calibration standpoint.

Deep Neural Network Calibration Calibration aligns a model’s correctness with its confidence estimates. Relevant examples of different calibration methods include; (a) Confidence penalizers that restrict model confidences [7, 16, 34, 35, 42, 46, 47]. (b) Regularizers that interpolate the model’s loss optimization space [13, 49, 53, 70]. For this work, VORD draws inspiration from the confidence penalty-regularizer techniques in (a) and (b) to deliver well-calibrated ordinal LVLM predictions.

3. Background and Motivation

3.1. Preliminaries

We begin by considering a decoding problem for a LVLM parameterized by θ . Given an input textual prompt x and input visual context v , the LVLM is simply a mapping $P_\theta : X, V \rightarrow Y$ between the input vocabulary & visual space (X, V) to the predicted output token space Y . Fig. 4 illustrates a typical LVLM architecture, which mainly consists of three major components; a *vision encoder*, such as a vision transformer (ViT) denoted by f_θ , a *LLM* and a *projector* that connects the visual and text tokens from the two models. The goal of the LVLM is to autoregressively generate an appropriate response y sampled from the probability distribution conditioned on the textual query and visual context. Specifically:

$$y_t \sim P_\theta(y_t|v, x, y_{<t}) \propto \exp h_\theta(y_t|v, x, y_{<t}) \quad (1)$$

where y_t is the generated token at time step t , $y_{<t}$ represents the sequence of sampled tokens preceding y_t and h_θ are the logits obtained from the penultimate layer. The conditional probabilities of the model are obtained after the softmax function, which are then used to train the LVLM by maximizing the likelihoods of a valid sequence conditioned on the visual context and text prompt:

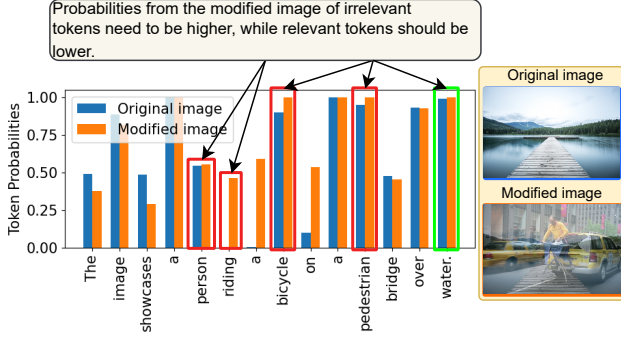


Figure 2. Comparisons between tokens probabilities obtained from the original and modified image. We observe a non-ordinal relations between both sets of probability distributions. The prompt used is: “Describe this image in detail.”

$\max_{\theta} \prod_{t=1}^T P_{\theta}(y_t | v, x, y_{<t})$. We consider a model perfectly calibrated if $\mathbb{P}(\hat{y} = y | \hat{P} = P) = P \quad \forall y \in P[0 - 1]$, whereby the predicted token confidence accurately reflects the probability of that token being correct. To measure calibration error, the commonly used metric is the expected calibration error (ECE) [48]:

$$ECE = \sum_{b=1}^B \frac{n_b}{N} |acc(b) - conf(b)|. \quad (2)$$

which divides predictions into B bins of n_b samples, measuring the weighted absolute difference between the average correctness $acc(b)$ and confidences $conf(b)$ of each bin.

A key challenge in calibrating LVLMs stems from the scarcity of target sequences. In ideal scenarios, we would have multiple examples of correct sequences for each input context and prompt, allowing the model to calibrate the assigned confidences of each token [73]. Unfortunately, most visual question answering training datasets only have a single target sequence per input, making it difficult to obtain well-calibrated predictions. Recent studies [38, 41, 52, 73] have proposed two-stage methods that involves the generation and re-ranking of token candidates for LLMs. Our work closely aligns with this line of research, but from a vision-based perspective for LVLMs.

3.2. Why do LVLMs Hallucinate?

Object hallucinations in LVLMs can largely be attributed to various reasons, such as: (1) Statistical imbalances and object correlations of the training corpus [1, 2, 4, 15, 77] which can cause the model to generate references to objects with higher occurrences in the training data. (2) Intrinsic biases and over-reliance on textual priors ingrained within the large language model [11, 26, 30, 67], resulting in the model prioritizing textual consistency as opposed to factual consistency. (3) Model’s inability to accurately differentiate context from facts during the generation process [6],

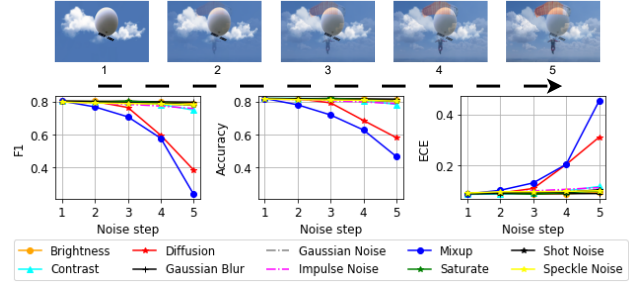


Figure 3. Visual corruptions, such as random noise and image mixing can introduce uncertainty into LVLMs. Our findings indicate that Mixup can be a particularly effective technique for inducing uncertainty, leading to more significant errors than diffusion noise.

which can lead to the inclusion of irrelevant or erroneous details. Recent studies indicate that hallucinations are not random, but follow certain patterns and tendencies such as the propensity to generate common objects or those closely related to the generated text [22, 77].

3.3. Inducing Visual Uncertainties in LVLMs

The visual quality of images fed into LVLMs directly impacts their generative abilities and faithfulness. If these input images are corrupted, it can lead to errors in the model’s output. Recent studies have shown that by inducing visual uncertainties *e.g.* Diffusion noise [3, 26] into the input images, LVLMs are more likely to generate incorrect/hallucinatory descriptions.

These visual uncertainties can cause the model to develop a propensity to generate common objects that frequently appear in the training data [30, 77], neglecting important visual context cues. In other words, LVLMs may prioritize generating familiar or expected textual content over accurately representing the visual context, especially when confronted with visual uncertainty. Fig. 3 shows the sensitivity of LVLMs to different visual corruption types such as Contrast and Brightness [17], with Diffusion noise and Mixup causing significant performance drops. While a detailed analysis of different corruption types is beyond the scope of this work, we include additional ablation studies on different corruptions in Appendix B.

3.4. Do LVLMs Hallucinate Ordinally?

Although recent studies have explored the effects of visual uncertainties on LVLMs and how contrasting generated tokens can help alleviate hallucinations. An interesting question remains: Do LVLMs hallucinate ordinally under visual uncertainty? In other words, do the conditional probabilities of generated tokens consistently follow a ranked order based on modifications to the given input?

To investigate this, we prompt a LVLM on different levels of modifications applied to the original image. These

modified images are presented to the LVLM to generate new and irrelevant outputs. An intriguing observation illustrated in Fig. 2, was that some tokens generated from the modified image \hat{v} do not always obey the expected transitive property, suggesting that LVLMs do not consistently hallucinate in a ranked ordinal pattern based on visual uncertainties. Specifically, tokens of interest from the clean image should ideally have higher probabilities $P_\theta(y_t|v, x, y_{<t})$ than those from the modified image $P_\theta(y_t|\hat{v}, x, y_{<t})$ ¹. For the simple case with Mixup [70], we expect the following relationship to hold:

$$1.0 \geq \lambda_i \geq \lambda_j \Leftrightarrow P_\theta(y_t|v, x) \geq P_\theta(y_t|\hat{v}, x) \quad (3)$$

Where $\lambda \in [0, 1] \sim \text{Beta}(\alpha, \alpha)$ is a hyperparameter randomly drawn from a Beta distribution and the modified sample obtained as: $\hat{v} = \lambda v_i + (1 - \lambda)v_j$. Our findings demonstrate that under the influence of Mixup, while undesirable tokens (in red) such as <person> and <bicycle> have higher probabilities than the original, making them easy to identify as hallucinations. On the other hand, desired tokens (in green) such as <water> should have much lower probabilities after modifications and did not behave as expected. To address this, we introduce VORD in the upcoming sections and also look at other variants of corruptions that can be used to induce visual uncertainties.

4. VORD: Visual Ordinal Calibration

Our findings in Sec. 3.4 demonstrate that under the influence of image corruptions, LVLMs do not follow a consistent relationship of token confidences. Leveraging off of this finding, we propose Visual Ordinal Calibration for calibrating LVLM text generations based on ordinal visual cues. VORD is designed to handle the negative influences of statistical biases and textual priors that lead to object hallucinations, while calibrating tokenwise confidences in an ordinal fashion. This section introduces VORD in two forms: 1.) a lightweight and cost-effective decoding variant and 2.) a learnable objective function for finetuning LVLMs. Lastly, we discuss our adaptive penalty margin used in both forms of VORD, based on the visual similarities between the original and modified image pairs.

4.1. Design 1: VORD Decoding

4.1.1. Visually Ordinal Tokens

The key principles of the transitive property in VORD can be utilized into a training-free decoding method. Given an original input image v , modified image \hat{v} and text prompt x , the model generates two sets of conditional probabilities based off $P_\theta(y_t|v, x, y_{<t})$ and $P_\theta(y_t|\hat{v}, x, y_{<t})$. We only

¹ For convenience in notation, we abbreviate $P_\theta(y_t|v, x, y_{<t})$ as $P_\theta(y_t|v, x)$ in the rest of this paper.

Algorithm 1: VORD - Visual Ordinal Decoding

Data: Given training corpus $D_{\text{train}} = (x_i, y_i)_{i=1}^N$

- 1: Initialize LVLM parameters θ
- 2: Begin: $y_0 = \text{BOS}, t = 1$
- 3: **while** $y_t \neq \text{EOS}$ **do**
- 4: $\hat{v} = \alpha * v_1 + (1 - \alpha) * v_2$ // Modify image
- 5: $m_\theta = \frac{1}{\pi} \arccos\left(\frac{\tilde{f}_\theta(v) \cdot \tilde{f}_\theta(\hat{v})}{\|\tilde{f}_\theta(v)\| \|\tilde{f}_\theta(\hat{v})\|}\right)$ // Sim margin
- 6: $\delta_\theta = P_\theta(y_t|v, x) + m_\theta \geq P_\theta(y_t|\hat{v}, x)$
- 7: $P_\theta^{\text{VORD}}(y_t|v, \hat{v}, x) = \begin{cases} P_\theta(y_t|v, x), & \text{if } \delta_\theta \\ 0, & \text{otherwise} \end{cases}$
- 8: $P_\theta^{\text{VORD}}(y_t|v, \hat{v}, x) = 0$, if $y_t \notin \mathcal{V}(y_{<t})$ // Eq. (5)
- 9: **return** $y_t \sim P_\theta^{\text{VORD}}(y_t|v, \hat{v}, x, y_{<t})$

consider tokens that have a higher probability than their counterparts generated from the modified image \hat{v} . VORD decoding is formalized as follows:

$$P_\theta^{\text{VORD}}(y|v, \hat{v}, x) = \begin{cases} P_\theta(y_t|v, x), & \text{accept, if } \delta_\theta \\ 0, & \text{otherwise reject} \end{cases} \quad (4)$$

where $\delta_\theta = P_\theta(y_t|v, x) + m_\theta \geq P_\theta(y_t|\hat{v}, x)$ is the ordinal mask that accepts/rejects tokens based on the transitive property of VORD, with the margin $m_\theta \in [0 - 1]$ controlling the stringency of acceptance. This condition ensures that the model prioritizes tokens that are consistent to the original image, mitigating the introduction of irrelevant or hallucinated elements. In scenarios where the modified image is visually equivalent to the original, the ordinal condition in Eq. (4) is not activated and VORD reduces to regular decoding. Subsequently, additional sampling strategies such as beam search [12], top-k sampling [10] and nucleus sampling [18] can also be performed together with VORD.

4.1.2. Adaptive Plausibility Constraints

The ordinal relationship in Eq. (4) may excessively penalize model outputs influenced by visually distorted inputs. Previous works have shown that although modified inputs tend to cause hallucinations, generated outputs often adhere to basic language rules and common sense [26]. VORD may inadvertently penalize valid outputs if the modified image generates a token with higher confidence than the original. To address this issue, we adopt the adaptive plausibility constraints used by [26, 29]:

$$\begin{aligned} \mathcal{V}(y_{<t}) &= \{y_t \in \mathcal{V} : \\ P_\theta(y_t|v, x, y_{<t}) &\geq \beta \max_w P_\theta(w|v, x, y_{<t})\}, \\ P_\theta^{\text{VORD}}(y_t|v, \hat{v}, x) &= 0, \text{ if } y_t \notin \mathcal{V}(y_{<t}), \end{aligned} \quad (5)$$

where \mathcal{V} represents the vocabulary of the LVLM and $\beta \in [0 - 1]$ is a hyperparameter controlling the strength of the

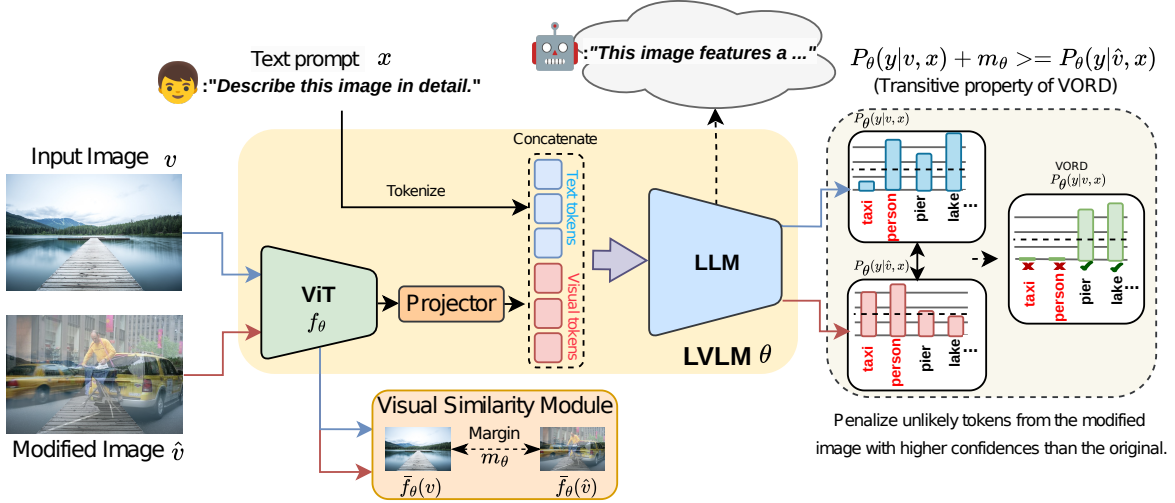


Figure 4. VORD penalizes tokens with higher conditional probabilities from \hat{v} than those from the original in v . The enforcement of the transitive property in VORD helps improve model performance, by filtering unlikely tokens during generation and training.

truncation of the next token. Higher values of β results more aggressive truncation, keeping only tokens with high confidence. The key steps for VORD decoding are summarized in Algorithm 1, which creates a modified image (e.g. Mixup or Diffusion), followed by computing the similarity margin Sec. 4.3 and performs VORD and adaptive plausibility constraints respectively.

4.2. Design 2: VORD Loss

Following the transitive property introduced in Eq. (3), we can derive a convex, piece-wise quadratic and differentiable loss function as follows:

$$\mathcal{L}_{\text{vord}} = \max(P_{\theta}(y|\hat{v}, x) - P_{\theta}(y|v, x) + m_{\theta}, 0)^{\psi} \quad (6)$$

where all tokens from the modified image with higher confidences than the original image, are penalized by a positive margin $m_{\theta} \geq 0$. The VORD loss can then be paired with the typical cross-entropy loss \mathcal{L} during model optimization using gradient descent, ensuring that the model not only generates accurate text descriptions but also maintains consistent ordinal relationships between tokens. The final objective for VORD loss is thus given by: $\mathcal{L}_{\text{CE}} + \mathcal{L}_{\text{vord}}$. Note that VORD loss is only a transitive condition enforced on the model’s probabilities and that the model does not directly learn on the modified images.

4.2.1. Gradient Analysis

We further discuss and analyze the VORD loss function, which can be broken down into the following two terms:

$$\mathcal{L}_{\text{vord}} = \begin{cases} (P_{\theta}(y|\hat{v}, x) - P_{\theta}(y|v, x) + m_{\theta})^{\psi}, & \text{if } g_{\theta} > 0 \\ 0, & \text{otherwise} \end{cases} \quad (7)$$

where $\psi > 0$ is a power term and the function $g_{\theta} = P_{\theta}(y|\hat{v}, x) - P_{\theta}(y|v, x) + m_{\theta}$ is the positive penalty obtained by the model for violating the transitive property in VORD. In contrast, the model is not penalized if the transitive property is obeyed.

First Derivative: Using the chain rule, we obtain novel gradients of $\mathcal{L}_{\text{vord}}$ in the following form:

$$\frac{\partial \mathcal{L}_{\text{vord}}}{\partial \theta} = \begin{cases} \psi g_{\theta}^{\psi-1} \frac{\partial g_{\theta}}{\partial \theta} & \text{if } g_{\theta} > 0 \\ 0, & \text{otherwise} \end{cases} \quad (8)$$

which is simply the difference between the gradients of the clean and modified images, multiplied by the positive penalty function g_{θ} . To further ensure that Eq. (6) is convex, we can compute the derivative of $\frac{\partial \mathcal{L}_{\text{vord}}}{\partial \theta}$.

Second Derivative: Using the product rule, the general form for the second derivative is obtained as:

$$\frac{\partial^2 \mathcal{L}_{\text{vord}}}{\partial^2 \theta} = \begin{cases} \psi g_{\theta}^{\psi-1} \frac{\partial^2 g_{\theta}}{\partial^2 \theta} + (\psi^2 - \psi) g_{\theta}^{\psi-2} \left(\frac{\partial g_{\theta}}{\partial \theta}\right)^2 & \text{if } g_{\theta} > 0 \\ 0, & \text{otherwise} \end{cases} \quad (9)$$

When $g_{\theta} > 0$ the second derivative is always positive, ensuring convexity. When $g_{\theta} \leq 0$ the second derivative is also zero, trivially indicating convexity. Therefore, the VORD loss in Eq. (6) is convex regardless of the value of g_{θ} .

4.3. Visual Similarities & Adaptive Penalty Margin

How do we effectively determine the penalty margin? In cases where differences between the original and modified images are small, naively over-penalizing the model by a fixed margin can lead to poor model performance. Furthermore, the manual assignment of the margin hyperparameter typically requires a cumbersome grid-search in order to obtain the optimal values of m_{θ} .

As an alternative, we propose a novel adaptive penalty margin based on visual angular similarities between pairs of original and

modified images. Consider the following function:

$$m_\theta = \frac{1}{\pi} \arccos \left(\frac{\bar{f}_\theta(v) \cdot \bar{f}_\theta(\hat{v})}{\|\bar{f}_\theta(v)\| \|\bar{f}_\theta(\hat{v})\|} \right) \quad (10)$$

where the cosine similarity is computed between the averaged original visual tokens $\bar{f}_\theta(v)$ and modified visual tokens $\bar{f}_\theta(\hat{v})$ extracted from the visual transformer f_θ . The margin $m_\theta \in [0 - 1]$ is then given by the inverse cosine similarity, normalized by π radians. This creates a general penalty margin that dynamically adjusts according to the level and type of noise in the modified image, ensuring appropriate penalization for any choice of image corruptions. Our proposed adaptive margin is designed to complement both VORD decoding and VORD loss, with Fig. 4 illustrating our entire workflow.

5. Experiments and Results

5.1. Datasets

POPE The Polling-based Object Probing Evaluation [30] benchmark queries the LVLm simple yes/no questions about whether certain specific objects exist in an input image. It uses a balanced set of questions (50-50 split of real and non-existent objects). There are three different settings used to determine non-existent objects: 1.) *Random*, when non-existent objects are chosen randomly. 2.) *Popular* where absent objects are selected from a list of commonly occurring objects and 3.) *Adversarial* where co-occurring objects not in the image are selected. The POPE dataset is constructed from three datasets, namely: MSCOCO [33], A-OKVQA [54], GQA [23]. We follow the evaluation protocols of other authors [26] and report model performance using standard evaluation metrics such as the accuracy, precision, recall, and F1 score.

MME Hallucination Subset This benchmark comprehensively evaluates various LVLm capabilities, including ten perception tasks and four cognition tasks. It includes subsets specifically designed to assess object-level hallucination (existence and count) and attribute-level hallucination (position and color). The MME dataset is built upon six preceding works: MSCOCO [33], MovieNet [21], Places [75], GoogleLandMarksV2 [64], Art500K [44] and CTW1500 [39]. Model performances are measured using the accuracy and “accuracy+” metrics.

LLaVA-Bench This LLaVA benchmark [36, 37] focuses on the LVLms’ ability to handle challenging tasks in various environments (indoor, outdoor, memes, paintings) and its ability to adapt to unseen domains. It includes 24 images comprising of 60 questions. We tailor specific case studies using the benchmark to qualitatively demonstrate the performances of different methods.

5.2. Models & Experiment Setup

We compare VORD Decoding against recently published methods, including VCD [26], OPERA beam search [22] and a baseline using regular decoding. For our evaluation on image question-answering benchmarks, we use LLaVA-v1.5 [37], Qwen-VL and InstructBLIP [8] backbone LVLms. For VORD loss, we perform

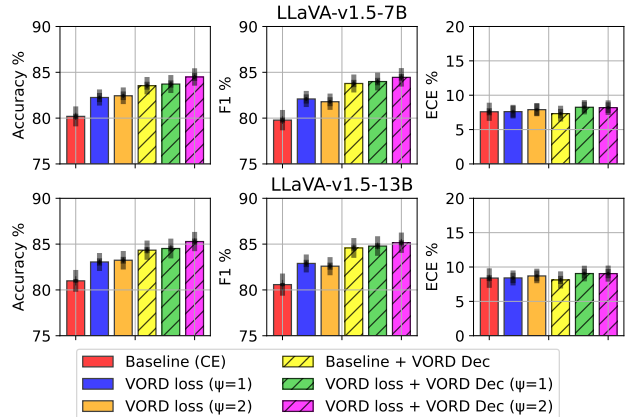


Figure 5. Our experiments demonstrate that finetuning LLaVA with VORD loss, particularly the squared variant ($\psi = 2$), highlighted in magenta, leads to consistent performance gains over the baseline. Moreover, combining VORD loss with VORD decoding (shaded) results in additional improvements.

instruction finetuning of LLaVA-v1.5 (7B and 13B) [37] initialized from pretrained Vicuna-v1.5 weights [58] and keep all hyperparameters on default as per detailed by [37]. We fix the number of bins as $B=15$ for the ECE. Our decoding experiments are evaluated on two NVIDIA A100 GPUs, while models trained with VORD loss are conducted on two NVIDIA H100 GPUs. More details on hyperparameters are included in Appendix A.1.

5.3. Experiment Results

Performance gains with VORD Loss We evaluate the effectiveness of our method by applying the transitive properties of VORD loss to fine-tune LoRA-adapted [19] backbone LVLm architectures; LLaVA-7B and LLaVA-13B [36] using our proposed VORD loss. Specifically, we compare the performance of a baseline model trained only with cross-entropy loss and models trained with VORD loss using different power terms ($\psi = 1$ and $\psi = 2$). Additionally, we show the performances of these models, when VORD decoding is further applied during inference.

Our results in Fig. 5 demonstrate that VORD loss yields significant improvements, particularly the squared variant ($\psi = 2$), by boosting accuracy and F1-score on the POPE hallucination benchmark by up to +2.9% and +2.7%, respectively, while maintaining good ECE throughout. Furthermore, combining VORD loss with VORD decoding results in additional gains, achieving the best overall performance. These improvements are consistent across both LLaVA-v1.5-7B and LLaVA-v1.5-13B. Additional results and discussions for VORD loss are presented in Appendix A.

Performance gains with VORD Decoding In Tab. 1, we compare our proposed VORD decoding against recently published baselines evaluated on the POPE benchmark. Our experiments demonstrate that VORD decoding achieves the state-of-the-art performance on the POPE benchmark, highlighting the effectiveness of VORD in mitigating object hallucinations. Specifically, we report consistent improvements over baseline methods by margins of up to +2.2% in accuracy and +2.3% in F1. Additionally, VORD

Datasets	Setting	Model	Method	Accuracy \uparrow	Precision \uparrow	Recall \uparrow	F1 \uparrow	ECE \downarrow
(Avg. scores of) MSCOCO + A-OKVQA + GQA	Random	LLaVA-v1.5	Regular	83.90 \pm 0.29	89.24 \pm 0.41	77.64 \pm 0.36	82.96 \pm 0.30	2.82 \pm 0.11
			OPERA	84.35 \pm 0.00	89.72 \pm 0.00	78.09 \pm 0.00	83.43 \pm 0.00	2.94 \pm 0.00
			VCD	86.17 \pm 0.22	90.76 \pm 0.11	81.07 \pm 0.43	85.54 \pm 0.26	7.35 \pm 0.10
			VORD (Ours)	88.35 \pm 0.32	90.59 \pm 0.33	86.01 \pm 0.30	88.18 \pm 0.32	2.69 \pm 0.09
		Qwen-VL	Regular	83.80 \pm 0.16	92.28 \pm 0.25	74.19 \pm 0.10	82.20 \pm 0.16	8.51 \pm 0.29
			OPERA	85.68 \pm 0.00	94.40 \pm 0.00	76.24 \pm 0.00	84.30 \pm 0.00	14.32 \pm 0.00
			VCD	85.51 \pm 0.09	92.74 \pm 0.01	77.43 \pm 0.23	84.34 \pm 0.13	11.53 \pm 0.07
			VORD (Ours)	85.87 \pm 0.13	93.69 \pm 0.28	77.33 \pm 0.21	84.67 \pm 0.14	7.56 \pm 0.14
		InstructBLIP	Regular	80.22 \pm 0.31	79.03 \pm 0.32	83.13 \pm 0.63	80.94 \pm 0.33	5.14 \pm 0.28
			OPERA	85.07 \pm 0.00	88.39 \pm 0.00	80.73 \pm 0.00	84.39 \pm 0.00	12.41 \pm 0.00
			VCD	83.30 \pm 0.22	82.93 \pm 0.11	84.70 \pm 0.30	83.66 \pm 0.21	6.69 \pm 0.23
			VORD (Ours)	84.19 \pm 0.25	84.37 \pm 0.65	84.70 \pm 0.45	84.41 \pm 0.18	2.95 \pm 0.03
	Popular	LLaVA-v1.5	Regular	80.27 \pm 0.52	82.50 \pm 0.56	77.45 \pm 0.56	79.72 \pm 0.54	3.14 \pm 0.04
			OPERA	81.04 \pm 0.00	83.36 \pm 0.00	78.16 \pm 0.00	80.50 \pm 0.00	3.23 \pm 0.00
			VCD	81.85 \pm 0.37	82.93 \pm 0.32	80.99 \pm 0.45	81.73 \pm 0.38	9.54 \pm 0.03
			VORD (Ours)	85.60 \pm 0.37	85.90 \pm 0.42	85.53 \pm 0.73	85.61 \pm 0.42	2.83 \pm 0.36
		Qwen-VL	Regular	81.70 \pm 0.35	87.53 \pm 0.33	74.45 \pm 0.46	80.34 \pm 0.39	9.09 \pm 0.34
			OPERA	83.02 \pm 0.00	90.61 \pm 0.00	76.24 \pm 0.00	82.71 \pm 0.00	15.98 \pm 0.00
			VCD	83.09 \pm 0.17	87.6 \pm 0.22	77.67 \pm 0.12	82.22 \pm 0.15	13.12 \pm 0.11
			VORD (Ours)	83.96 \pm 0.14	89.59 \pm 0.23	77.30 \pm 0.15	82.86 \pm 0.15	8.25 \pm 0.23
		InstructBLIP	Regular	76.04 \pm 0.31	73.00 \pm 0.50	83.33 \pm 0.24	77.70 \pm 0.20	8.48 \pm 0.33
			OPERA	78.33 \pm 0.00	73.85 \pm 0.00	87.73 \pm 0.00	80.20 \pm 0.00	14.90 \pm 0.00
			VCD	78.86 \pm 0.27	76.13 \pm 0.17	84.85 \pm 0.35	80.09 \pm 0.26	10.24 \pm 0.26
			VORD (Ours)	80.73 \pm 0.26	78.76 \pm 0.20	84.53 \pm 0.31	81.43 \pm 0.26	3.74 \pm 0.13
Adversarial	LLaVA-v1.5	Regular	76.39 \pm 0.38	76.36 \pm 0.34	77.42 \pm 0.55	76.68 \pm 0.40	5.63 \pm 0.09	
		OPERA	76.91 \pm 0.00	76.84 \pm 0.00	77.91 \pm 0.00	77.19 \pm 0.00	5.54 \pm 0.00	
		VCD	77.83 \pm 0.03	76.67 \pm 0.15	81.17 \pm 0.33	78.61 \pm 0.09	12.39 \pm 0.04	
		VORD (Ours)	80.72 \pm 0.71	78.51 \pm 0.63	85.27 \pm 1.02	81.60 \pm 0.73	4.57 \pm 0.30	
	Qwen-VL	Regular	79.46 \pm 0.06	82.94 \pm 0.10	74.73 \pm 0.13	78.47 \pm 0.08	10.86 \pm 0.13	
		OPERA	80.43 \pm 0.00	85.48 \pm 0.00	76.24 \pm 0.00	80.43 \pm 0.00	18.57 \pm 0.00	
		VCD	80.79 \pm 0.12	83.32 \pm 0.05	77.45 \pm 0.28	80.15 \pm 0.17	15.21 \pm 0.13	
		VORD (Ours)	81.22 \pm 0.11	84.22 \pm 0.22	77.45 \pm 0.16	80.52 \pm 0.07	10.09 \pm 0.06	
	InstructBLIP	Regular	72.71 \pm 0.27	69.21 \pm 0.29	82.99 \pm 0.25	75.31 \pm 0.21	11.11 \pm 0.27	
		OPERA	75.50 \pm 0.00	70.49 \pm 0.00	87.73 \pm 0.00	78.17 \pm 0.00	17.53 \pm 0.00	
		VCD	74.81 \pm 0.21	71.27 \pm 0.22	84.67 \pm 0.35	77.16 \pm 0.20	13.38 \pm 0.18	
		VORD (Ours)	76.77 \pm 0.35	73.67 \pm 0.41	84.51 \pm 0.17	78.51 \pm 0.30	6.82 \pm 0.05	

Table 1. We report the averaged results (%) of reruns for different methods evaluated on all three datasets of the POPE benchmark. VORD decoding effectively mitigates object hallucinations, while better calibrating model predictions.

exhibits better calibration, as evidenced by the best ECE scores on LLaVA, QWEN and InstructBLIP.

Furthermore, all LVLMs exhibit a significant performance decline when transitioning from random to popular and adversarial settings. In contrast, VORD remains relatively robust, even in the highly challenging adversarial subset. Additionally, Tab. 2 presents a comparative analysis of various methods on the MME perception benchmark. While improvements vary across individual tasks, we observe significant gains over regular decoding in overall performance for LLaVA, QWEN, and InstructBLIP of 7.6%, 5.5%, and 15.9% respectively. Notably, VORD achieves the highest results overall securing the top performance and calibration on all architectures. Individual scores of each method are detailed in Appendix A.

6. Discussion and Analysis

Evaluation and Analysis on LLaVA-Bench We further examine VORD’s performance on complex open-ended VQA tasks, using LLaVA-Bench. We adopt the evaluation protocol of [26, 69] and select the latest LVLM model GPT4oV as a third party evaluator. For our assessment, we specifically prompt each backbone LVLM with “Describe this image in detail.” for every image. We then consolidate the responses of each decoding method

Model	Method	Perception \uparrow	Recognition \uparrow	Overall Scores \uparrow
LLaVA-v1.5	Regular	1294.86 \pm 21.20	331.19 \pm 15.05	1626.05 \pm 28.82
	VCD	1356.27 \pm 20.05	309.04 \pm 21.89	1665.32 \pm 33.45
	OPERA	1332.79 \pm 0.00	330.71 \pm 0.00	1663.50 \pm 0.00
	VORD (Ours)	1393.75 \pm 20.29	334.04 \pm 20.77	1727.79 \pm 32.47
Qwen-VL	Regular	1352.50 \pm 21.31	313.04 \pm 16.40	1665.54 \pm 36.62
	VCD	1403.17 \pm 14.57	318.13 \pm 22.77	1721.30 \pm 36.16
	OPERA	1400.37 \pm 25.86	271.78 \pm 31.20	1672.15 \pm 42.66
	VORD (Ours)	1427.07 \pm 22.90	314.28 \pm 21.75	1741.36 \pm 36.73
InstructBLIP	Regular	976.99 \pm 27.70	276.42 \pm 17.10	1253.42 \pm 28.26
	VCD	1088.80 \pm 28.58	292.50 \pm 18.16	1381.30 \pm 30.64
	OPERA	1044.80 \pm 0.00	270.35 \pm 0.00	1315.15 \pm 0.00
	VORD (Ours)	1132.98 \pm 29.06	271.54 \pm 12.93	1404.52 \pm 32.74

Table 2. We report the main results (%) comparing different methods computed across 3 seeds, evaluated on the MME benchmark. VORD decoding delivers the best overall performance.

and score individual responses on GPT4oV using a prompt card (see Appendix C). GPT4oV is tasked to rate the accuracy and detailedness of responses, paying extra attention to any hallucinations in the generations. Accuracy refers to the correctness of the response, while Detailedness measures how informative each response is. Tab. 3 shows that VORD consistently produces highly accurate and detailed responses across all three baseline models,

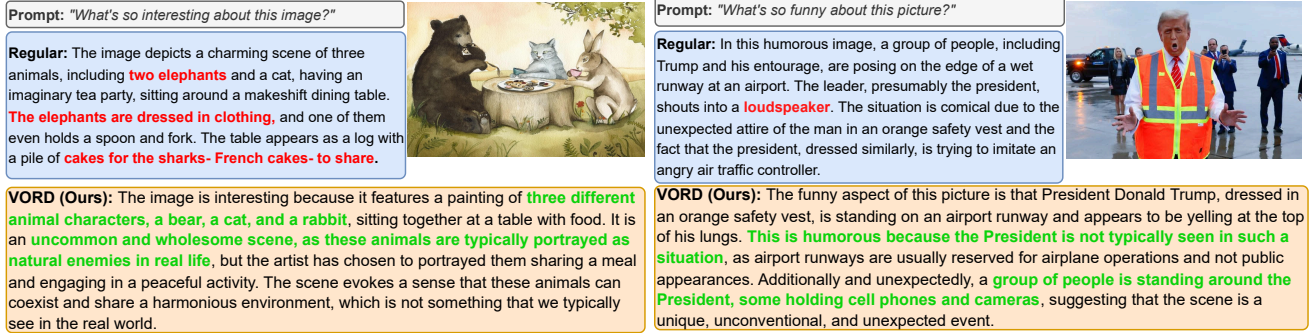


Figure 6. VORD produces accurate and detailed outputs, mitigating object hallucinations across a wide range of different visual cues. Hallucinations are in red, while accurate and detailed responses are in green.

Model	Method	Avg Lengths	Accuracy \uparrow	Detailedness \uparrow
LLaVA-1.5	Regular	97.02 \pm 2.78	4.41	4.75
	VCD	97.93 \pm 3.98	5.20	5.50
	VORD	91.61 \pm 6.32	5.88	5.92
InstructBLIP	Regular	102.21 \pm 1.20	3.39	3.83
	VCD	104.00 \pm 1.04	4.17	4.69
	VORD	97.91 \pm 1.15	4.65	4.70
Qwen-VL	Regular	10.41 \pm 1.21	7.28	6.09
	VCD	10.36 \pm 1.15	7.30	6.76
	VORD	13.13 \pm 1.62	8.86	6.95

Table 3. Evaluation results from GPT-4oV comparing the open-ended responses for different methods. Accuracy and Detailedness are gauged on a scale of 10. VORD delivers short but accurate and detailed responses.

demonstrating its effectiveness in tackling complex VQA tasks.

Length of token generations (Short & Sweet) A concept known as Occam’s Razor states that when you have two choices that are equally good, the simpler one is usually better. Building on this principle, we explore how VORD generates shorter text outputs by comparing the average token generation lengths of regular decoding, VCD, and VORD on LLaVA-Bench. Tab. 3 shows that VORD has average shorter token generation lengths, whilst achieving the highest accuracy and detailedness.

Delving deeper, we analyze two case studies in Fig. 6. In the first case, regular decoding hallucinates potentially present objects like `<elephants>` and `<cakes>`, whereas VORD accurately identifies the three distinct animals in the image. In the second case involving an image of Trump, regular decoding hallucinates the object `<loudspeaker>`, whereas VORD accurately captures the uniqueness of President Trump’s antics.

Effects of Margin Parameter We perform an ablation study to evaluate the influence of our proposed adaptive visual similarity margin on VORD decoding. Specifically, we compare our method against regular decoding and four fixed margin settings: $m_\theta = [0.00, 0.25, 0.50, 0.75]$ using LLaVA-v1.5 on the MME benchmark. Tab. 4 shows that VORD decoding without a margin ($m_\theta = 0.0$), struggles to differentiate tokens between original and

m_θ	Perception \uparrow	Recognition \uparrow	Overall Scores \uparrow
Regular	1294.86 \pm 21.20	331.19 \pm 15.05	1626.05 \pm 28.82
0.00	1172.51 \pm 15.54	245.71 \pm 21.55	1418.23 \pm 30.68
0.25	1376.61 \pm 20.87	342.85 \pm 18.68	1719.46 \pm 31.09
0.50	1356.23 \pm 22.72	351.25 \pm 16.80	1707.48 \pm 30.26
0.75	1336.50 \pm 23.50	350.89 \pm 16.67	1687.39 \pm 30.07
Adaptive (Ours)	1393.75 \pm 20.29	334.04 \pm 20.77	1727.79 \pm 32.47

Table 4. Comparisons of different margin settings for VORD decoding evaluated on MME. Our proposed adaptive visual similarity margin delivers the best performance.

modified images, leading to weaker performance than regular decoding. Conversely, excessively large margins ($m_\theta > 0.25$) can over-penalize predictions, degrading performance. Our proposed adaptive margin, which eliminates the need for hyperparameter tuning, achieves the best overall performance. Additional ablation studies on the effects of various visual corruptions are included in Appendix B.

7. Limitations

While this work primarily focuses on mitigating object hallucinations in LVLMS, we believe that the transitive property of VORD can be extended to LLMs and NLP. Although both VORD decoding and VORD loss currently rely on image modifications, we envision future adaptations involving text or ground truth label modifications. This would enable VORD to address hallucinations in a broader range of applications.

8. Conclusion

We present VORD, visual ordinal calibration for LVLMS. VORD is proposed in two forms: a training-free contrastive decoding method and a novel ordinal ranking loss function. VORD also utilizes an adaptive visual similarity margin, which dynamically computes a penalty margin based on the visual similarities between original and modified images. Our experiments demonstrate VORD’s effectiveness in mitigating object hallucinations and delivering well-calibrated confidence estimates in LVLMS.

References

- [1] Vedika Agarwal, Rakshith Shetty, and Mario Fritz. Towards causal vqa: Revealing and reducing spurious correlations by invariant and covariant semantic editing. In *IEEE/CVF Conference on Computer Vision and Pattern Recognition (CVPR)*, 2020. 3
- [2] Aishwarya Agrawal, Dhruv Batra, and Devi Parikh. Analyzing the behavior of visual question answering models. In *Proceedings of the 2016 Conference on Empirical Methods in Natural Language Processing*, pages 1955–1960, Austin, Texas, 2016. Association for Computational Linguistics. 3
- [3] Wenbin An, Feng Tian, Sicong Leng, Jiahao Nie, Haonan Lin, Qianying Wang, Guang Dai, Ping Chen, and Shijian Lu. Aqla: Mitigating object hallucinations in large vision-language models with assembly of global and local attention. *ArXiv, abs/2406.12718*, 2024. 3
- [4] Ali Furkan Biten, Luís Gómez, and Dimosthenis Karatzas. Let there be a clock on the beach: Reducing object hallucination in image captioning. In *Proceedings of the IEEE/CVF Winter Conference on Applications of Computer Vision (WACV)*, pages 1381–1390, 2022. 3
- [5] Long Chen, Oleg Sinavski, Jan Hünermann, Alice Karnsund, Andrew James Willmott, Danny Birch, Daniel Maund, and Jamie Shotton. Driving with llms: Fusing object-level vector modality for explainable autonomous driving. In *2024 IEEE International Conference on Robotics and Automation (ICRA)*, 2024. 1
- [6] Zhaorun Chen, Zhuokai Zhao, Hongyin Luo, Huaxiu Yao, Bo Li, and Jiawei Zhou. HALC: Object hallucination reduction via adaptive focal-contrast decoding. In *Proceedings of the 41st International Conference on Machine Learning*, pages 7824–7846. PMLR, 2024. 2, 3
- [7] Jiacheng Cheng and Nuno Vasconcelos. Calibrating deep neural networks by pairwise constraints. In *Proceedings of the IEEE/CVF Conference on Computer Vision and Pattern Recognition (CVPR)*, pages 13709–13718, 2022. 2
- [8] Wenliang Dai, Junnan Li, Dongxu Li, Anthony Tiong, Junqi Zhao, Weisheng Wang, Boyang Li, Pascale Fung, and Steven Hoi. InstructBLIP: Towards general-purpose vision-language models with instruction tuning. In *Thirty-seventh Conference on Neural Information Processing Systems*, 2023. 6
- [9] Jacob Devlin, Ming-Wei Chang, Kenton Lee, and Kristina Toutanova. BERT: Pre-training of deep bidirectional transformers for language understanding. In *Proceedings of the 2019 Conference of the North American Chapter of the Association for Computational Linguistics: Human Language Technologies, Volume 1 (Long and Short Papers)*, pages 4171–4186, Minneapolis, Minnesota, 2019. Association for Computational Linguistics. 2
- [10] Angela Fan, Mike Lewis, and Yann Dauphin. Hierarchical neural story generation. In *Proceedings of the 56th Annual Meeting of the Association for Computational Linguistics (Volume 1: Long Papers)*, pages 889–898, Melbourne, Australia, 2018. Association for Computational Linguistics. 4
- [11] Alessandro Favero, Luca Zancato, Matthew Trager, Siddharth Choudhary, Pramuditha Perera, Alessandro Achille, Ashwin Swaminathan, and Stefano Soatto. Multi-modal hallucination control by visual information grounding. In *Proceedings of the IEEE/CVF Conference on Computer Vision and Pattern Recognition (CVPR)*, pages 14303–14312, 2024. 1, 2, 3
- [12] Markus Freitag and Yaser Al-Onaizan. Beam search strategies for neural machine translation. In *Proceedings of the First Workshop on Neural Machine Translation*, pages 56–60, Vancouver, 2017. Association for Computational Linguistics. 4
- [13] Yarín Gal and Zoubin Ghahramani. Dropout as a bayesian approximation: Representing model uncertainty in deep learning. In *Proceedings of The 33rd International Conference on Machine Learning*, pages 1050–1059, New York, New York, USA, 2016. PMLR. 2
- [14] Ido Galil, Mohammed Dabbah, and Ran El-Yaniv. What can we learn from the selective prediction and uncertainty estimation performance of 523 imagenet classifiers? In *The Eleventh International Conference on Learning Representations*, 2023. 2
- [15] Yash Goyal, Tejas Khot, Douglas Summers-Stay, Dhruv Batra, and Devi Parikh. Making the v in vqa matter: Elevating the role of image understanding in visual question answering. In *Proceedings of the IEEE Conference on Computer Vision and Pattern Recognition (CVPR)*, 2017. 3
- [16] Ramya Hebbalaguppe, Jatin Prakash, Neelabh Madan, and Chetan Arora. A stitch in time saves nine: A train-time regularizing loss for improved neural network calibration. In *Proceedings of the IEEE/CVF Conference on Computer Vision and Pattern Recognition (CVPR)*, pages 16081–16090, 2022. 2
- [17] Dan Hendrycks and Thomas G. Dietterich. Benchmarking neural network robustness to common corruptions and perturbations. In *7th International Conference on Learning Representations, ICLR 2019, New Orleans, LA, USA, May 6-9, 2019*. OpenReview.net, 2019. 3, 13
- [18] Ari Holtzman, Jan Buys, Li Du, Maxwell Forbes, and Yejin Choi. The curious case of neural text degeneration. In *International Conference on Learning Representations*, 2020. 4
- [19] Edward J Hu, Yelong Shen, Phillip Wallis, Zeyuan Allen-Zhu, Yuanzhi Li, Shean Wang, Lu Wang, and Weizhu Chen. LoRA: Low-rank adaptation of large language models. In *International Conference on Learning Representations*, 2022. 6
- [20] Xiaowei Hu, Zhe Gan, Jianfeng Wang, Zhengyuan Yang, Zicheng Liu, Yumao Lu, and Lijuan Wang. Scaling up vision-language pre-training for image captioning. In *Proceedings of the IEEE/CVF Conference on Computer Vision and Pattern Recognition (CVPR)*, pages 17980–17989, 2022. 1
- [21] Qingqiu Huang, Yu Xiong, Anyi Rao, Jiaze Wang, and Dahua Lin. Movienet: A holistic dataset for movie understanding. In *European Conference on Computer Vision*, 2020. 6

- [22] Qidong Huang, Xiaoyi Dong, Pan Zhang, Bin Wang, Conghui He, Jiaqi Wang, Dahua Lin, Weiming Zhang, and Nenghai Yu. Opera: Alleviating hallucination in multimodal large language models via over-trust penalty and retrospection-allocation. In *Proceedings of the IEEE/CVF Conference on Computer Vision and Pattern Recognition (CVPR)*, pages 13418–13427, 2024. 1, 2, 3, 6
- [23] Drew A. Hudson and Christopher D. Manning. Gqa: A new dataset for real-world visual reasoning and compositional question answering. In *Proceedings of the IEEE/CVF Conference on Computer Vision and Pattern Recognition (CVPR)*, 2019. 6
- [24] Zixia Jia, Mengmeng Wang, Baichen Tong, and Zilong Zheng. Langsuit-e: Controlling, planning, and interacting with large language models in embodied text environments. In *Findings of the 62nd Annual Meeting of the Association for Computational Linguistics (ACL 2024)*, 2024. 1
- [25] Adam Tauman Kalai and Santosh S. Vempala. Calibrated language models must hallucinate. *Proceedings of the 56th Annual ACM Symposium on Theory of Computing*, 2023. 2
- [26] Sicong Leng, Hang Zhang, Guanzheng Chen, Xin Li, Shijian Lu, Chunyan Miao, and Lidong Bing. Mitigating object hallucinations in large vision-language models through visual contrastive decoding. In *Proceedings of the IEEE/CVF Conference on Computer Vision and Pattern Recognition (CVPR)*, pages 13872–13882, 2024. 1, 2, 3, 4, 6, 7
- [27] Junnan Li, Dongxu Li, Caiming Xiong, and Steven Hoi. BLIP: Bootstrapping language-image pre-training for unified vision-language understanding and generation. In *Proceedings of the 39th International Conference on Machine Learning*, pages 12888–12900. PMLR, 2022. 2
- [28] Liunian Harold Li, Mark Yatskar, Da Yin, Cho-Jui Hsieh, and Kai-Wei Chang. What does BERT with vision look at? In *Proceedings of the 58th Annual Meeting of the Association for Computational Linguistics*, pages 5265–5275, Online, 2020. Association for Computational Linguistics. 2
- [29] Xiang Lisa Li, Ari Holtzman, Daniel Fried, Percy Liang, Jason Eisner, Tatsunori Hashimoto, Luke Zettlemoyer, and Mike Lewis. Contrastive decoding: Open-ended text generation as optimization. In *Proceedings of the 61st Annual Meeting of the Association for Computational Linguistics (Volume 1: Long Papers)*, pages 12286–12312, Toronto, Canada, 2023. Association for Computational Linguistics. 4
- [30] Yifan Li, Yifan Du, Kun Zhou, Jinpeng Wang, Xin Zhao, and Ji-Rong Wen. Evaluating object hallucination in large vision-language models. In *Proceedings of the 2023 Conference on Empirical Methods in Natural Language Processing*, pages 292–305, Singapore, 2023. Association for Computational Linguistics. 3, 6
- [31] Ji Lin, Hongxu Yin, Wei Ping, Pavlo Molchanov, Mohammad Shoeybi, and Song Han. Vila: On pre-training for visual language models. In *Proceedings of the IEEE/CVF Conference on Computer Vision and Pattern Recognition (CVPR)*, pages 26689–26699, 2024. 2
- [32] Stephanie Lin, Jacob Hilton, and Owain Evans. TruthfulQA: Measuring how models mimic human falsehoods. In *Proceedings of the 60th Annual Meeting of the Association for Computational Linguistics (Volume 1: Long Papers)*, pages 3214–3252, Dublin, Ireland, 2022. Association for Computational Linguistics. 2
- [33] Tsung-Yi Lin, Michael Maire, Serge J. Belongie, James Hays, Pietro Perona, Deva Ramanan, Piotr Dollár, and C. Lawrence Zitnick. Microsoft coco: Common objects in context. In *European Conference on Computer Vision*, 2014. 6
- [34] Bingyuan Liu, Ismail Ben Ayed, Adrian Galdran, and Jose Dolz. The devil is in the margin: Margin-based label smoothing for network calibration. In *Proceedings of the IEEE/CVF Conference on Computer Vision and Pattern Recognition (CVPR)*, pages 80–88, 2022. 2
- [35] Bingyuan Liu, Jérôme Rony, Adrian Galdran, Jose Dolz, and Ismail Ben Ayed. Class adaptive network calibration. In *Proceedings of the IEEE/CVF Conference on Computer Vision and Pattern Recognition (CVPR)*, pages 16070–16079, 2023. 2
- [36] Haotian Liu, Chunyuan Li, Qingyang Wu, and Yong Jae Lee. Visual instruction tuning. In *Advances in Neural Information Processing Systems*, pages 34892–34916. Curran Associates, Inc., 2023. 2, 6
- [37] Haotian Liu, Chunyuan Li, Yuheng Li, and Yong Jae Lee. Improved baselines with visual instruction tuning. In *Proceedings of the IEEE/CVF Conference on Computer Vision and Pattern Recognition (CVPR)*, pages 26296–26306, 2024. 2, 6
- [38] Yixin Liu and Pengfei Liu. SimCLS: A simple framework for contrastive learning of abstractive summarization. In *Proceedings of the 59th Annual Meeting of the Association for Computational Linguistics and the 11th International Joint Conference on Natural Language Processing (Volume 2: Short Papers)*, pages 1065–1072, Online, 2021. Association for Computational Linguistics. 3
- [39] Yuliang Liu, Lianwen Jin, Shuaitao Zhang, Canjie Luo, and Sheng Zhang. Curved scene text detection via transverse and longitudinal sequence connection. *Pattern Recognition*, 90: 337–345, 2019. 6
- [40] Yinhan Liu, Myle Ott, Naman Goyal, Jingfei Du, Mandar Joshi, Danqi Chen, Omer Levy, Mike Lewis, Luke Zettlemoyer, and Veselin Stoyanov. Roberta: A robustly optimized bert pretraining approach, 2019. 2
- [41] Yixin Liu, Pengfei Liu, Dragomir Radev, and Graham Neubig. BRIO: Bringing order to abstractive summarization. In *Proceedings of the 60th Annual Meeting of the Association for Computational Linguistics (Volume 1: Long Papers)*, pages 2890–2903, Dublin, Ireland, 2022. Association for Computational Linguistics. 3
- [42] Yang Liu, Shen Yan, Laura Leal-Taixé, James Hays, and Deva Ramanan. Soft augmentation for image classification. In *Proceedings of the IEEE/CVF Conference on Computer Vision and Pattern Recognition (CVPR)*, pages 16241–16250, 2023. 2
- [43] Yingzi Ma, Yulong Cao, Jiachen Sun, Marco Pavone, and Chaowei Xiao. Dolphins: Multimodal language model for driving, 2023. 1
- [44] Hui Mao, Ming Cheung, and James She. Deepart: Learning joint representations of visual arts. In *Proceedings of*

- the 25th ACM International Conference on Multimedia*, page 1183–1191, New York, NY, USA, 2017. Association for Computing Machinery. 6
- [45] Matthias Minderer, Josip Djolonga, Rob Romijnders, Frances Hubis, Xiaohua Zhai, Neil Houlsby, Dustin Tran, and Mario Lucic. Revisiting the calibration of modern neural networks. In *Advances in Neural Information Processing Systems*, pages 15682–15694. Curran Associates, Inc., 2021. 2
- [46] Jooyoung Moon, Jihyo Kim, Younghak Shin, and Sangheum Hwang. Confidence-aware learning for deep neural networks. In *Proceedings of the 37th International Conference on Machine Learning*, pages 7034–7044. PMLR, 2020. 2
- [47] Rafael Müller, Simon Kornblith, and Geoffrey E Hinton. When does label smoothing help? In *Advances in Neural Information Processing Systems*. Curran Associates, Inc., 2019. 2
- [48] Mahdi Pakdaman Naeini, Gregory F. Cooper, and Milos Hauskrecht. Obtaining well calibrated probabilities using bayesian binning. In *Proceedings of the Twenty-Ninth AAAI Conference on Artificial Intelligence*, page 2901–2907. AAAI Press, 2015. 3
- [49] Jongyoun Noh, Hyekang Park, Junghyup Lee, and Bumsuh Ham. Rankmixup: Ranking-based mixup training for network calibration. In *Proceedings of the IEEE/CVF International Conference on Computer Vision (ICCV)*, pages 1358–1368, 2023. 2
- [50] Sandhini Agarwal OpenAI: Josh Achiam, Steven Adler and Lama Ahmad et al. Gpt-4 technical report. In *ChatGPT4 Report*, 2023. 2
- [51] Alec Radford, Jong Wook Kim, Chris Hallacy, Aditya Ramesh, Gabriel Goh, Sandhini Agarwal, Girish Sastry, Amanda Askell, Pamela Mishkin, Jack Clark, Gretchen Krueger, and Ilya Sutskever. Learning transferable visual models from natural language supervision. In *Proceedings of the 38th International Conference on Machine Learning*, pages 8748–8763. PMLR, 2021. 2
- [52] Mathieu Ravaut, Shafiq Joty, and Nancy Chen. SummaRanker: A multi-task mixture-of-experts re-ranking framework for abstractive summarization. In *Proceedings of the 60th Annual Meeting of the Association for Computational Linguistics (Volume 1: Long Papers)*, pages 4504–4524, Dublin, Ireland, 2022. Association for Computational Linguistics. 3
- [53] Hitesh Sapkota, Dingrong Wang, Zhiqiang Tao, and Qi Yu. Distributionally robust ensemble of lottery tickets towards calibrated sparse network training. In *Advances in Neural Information Processing Systems*, pages 62657–62681. Curran Associates, Inc., 2023. 2
- [54] Dustin Schwenk, Apoorv Khandelwal, Christopher Clark, Kenneth Marino, and Roozbeh Mottaghi. A-okvqa: A benchmark for visual question answering using world knowledge. In *European Conference on Computer Vision*, 2022. 6
- [55] Weijia Shi, Sewon Min, Michihiro Yasunaga, Minjoon Seo, Richard James, Mike Lewis, Luke Zettlemoyer, and Wentaoh Yih. REPLUG: Retrieval-augmented black-box language models. In *Proceedings of the 2024 Conference of the North American Chapter of the Association for Computational Linguistics: Human Language Technologies (Volume 1: Long Papers)*, pages 8371–8384, Mexico City, Mexico, 2024. Association for Computational Linguistics. 2
- [56] Chen Sun, Austin Myers, Carl Vondrick, Kevin Murphy, and Cordelia Schmid. Videobert: A joint model for video and language representation learning. In *Proceedings of the IEEE/CVF International Conference on Computer Vision (ICCV)*, 2019. 2
- [57] Guohao Sun, Can Qin, Jiamian Wang, Zeyuan Chen, Ran Xu, and Zhiqiang Tao. Sq-llava: Self-questioning for large vision-language assistant. In *ECCV*, 2024. 2
- [58] Hugo Touvron, Thibaut Lavril, Gautier Izacard, Xavier Martinet, Marie-Anne Lachaux, Timothée Lacroix, Baptiste Rozière, Naman Goyal, Eric Hambro, Faisal Azhar, Aurelien Rodriguez, Armand Joulin, Edouard Grave, and Guillaume Lample. Llama: Open and efficient foundation language models. *ArXiv*, abs/2302.13971, 2023. 2, 6
- [59] Weijie Tu, Weijian Deng, and Tom Gedeon. A closer look at the robustness of contrastive language-image pre-training (clip). In *Advances in Neural Information Processing Systems*, pages 13678–13691. Curran Associates, Inc., 2023. 2
- [60] Weijie Tu, Weijian Deng, Dylan Campbell, Stephen Gould, and Tom Gedeon. An empirical study into what matters for calibrating vision-language models. In *Proceedings of the 41st International Conference on Machine Learning*, pages 48791–48808. PMLR, 2024. 2
- [61] Jianfeng Wang, Zhengyuan Yang, Xiaowei Hu, Linjie Li, Kevin Lin, Zhe Gan, Zicheng Liu, Ce Liu, and Lijuan Wang. GIT: A generative image-to-text transformer for vision and language. *Transactions on Machine Learning Research*, 2022. 2
- [62] Sheng Wang, Zihao Zhao, Xi Ouyang, Qian Wang, and Dinggang Shen. Chatcad: Interactive computer-aided diagnosis on medical image using large language models. *arXiv preprint arXiv:2302.07257*, 2023. 1
- [63] Yuxi Wei, Zi Wang, Yifan Lu, Chenxin Xu, Changxing Liu, Hao Zhao, Siheng Chen, and Yanfeng Wang. Editable scene simulation for autonomous driving via collaborative llm-agents. In *Proceedings of the IEEE/CVF Conference on Computer Vision and Pattern Recognition (CVPR)*, pages 15077–15087, 2024. 1
- [64] Tobias Weyand, Andre Araujo, Bingyi Cao, and Jack Sim. Google landmarks dataset v2 - a large-scale benchmark for instance-level recognition and retrieval. In *IEEE/CVF Conference on Computer Vision and Pattern Recognition (CVPR)*, 2020. 6
- [65] Yiquan Wu, Siying Zhou, Yifei Liu, Weiming Lu, Xiaozhong Liu, Yating Zhang, Changlong Sun, Fei Wu, and Kun Kuang. Precedent-enhanced legal judgment prediction with LLM and domain-model collaboration. In *The 2023 Conference on Empirical Methods in Natural Language Processing*, 2023. 1
- [66] Weijia Xu, Sweta Agrawal, Eleftheria Briakou, Marianna J. Martindale, and Marine Carpuat. Understanding and detecting hallucinations in neural machine translation via model introspection. *Transactions of the Association for Computational Linguistics*, 11:546–564, 2023. 2

- [67] Qinghao Ye, Haiyang Xu, Guohai Xu, Jiabo Ye, Ming Yan, Yi Zhou, Junyan Wang, Anwen Hu, Pengcheng Shi, Yaya Shi, Chenliang Li, Yuanhong Xu, Hehong Chen, Junfeng Tian, Qiang Qi, Ji Zhang, and Feiyan Huang. mplug-owl: Modularization empowers large language models with multimodality. *ArXiv*, abs/2304.14178, 2023. [3](#)
- [68] Nur Yildirim, Hannah Richardson (nee Murfet), Maria T Wetscherek, Junaid Bajwa, Joseph Jacob, Mark A Pinnock, Stephen Harris, Daniel Coelho de Castro, Shruthi Bannur, Stephanie Hyland, Pratik Ghosh, Mercy Ranjit, Kenza Bouzid, Anton Schwaighofer, Fernando Pérez-García, Harshita Sharma, Ozan Oktay, Matthew P Lungren, Javier Alvarez-Valle, Aditya Nori, and Anja Thieme. Multimodal healthcare ai: Identifying and designing clinically relevant vision-language applications for radiology. In *CHI 2024*. ACM, 2024. [1](#)
- [69] Shukang Yin, Chaoyou Fu, Sirui Zhao, Tong Xu, Hao Wang, Dianbo Sui, Yunhang Shen, Ke Li, Xingguo Sun, and Enhong Chen. Woodpecker: Hallucination correction for multimodal large language models. *ArXiv*, abs/2310.16045, 2023. [1](#), [2](#), [7](#)
- [70] Hongyi Zhang, Moustapha Cissé, Yann N. Dauphin, and David Lopez-Paz. mixup: Beyond empirical risk minimization. In *6th International Conference on Learning Representations, ICLR 2018, Vancouver, BC, Canada, April 30 - May 3, 2018, Conference Track Proceedings*. OpenReview.net, 2018. [2](#), [4](#)
- [71] Letian Zhang, Xiaotong Zhai, Zhongkai Zhao, Yongshuo Zong, Xin Wen, and Bingchen Zhao. What if the tv was off? examining counterfactual reasoning abilities of multi-modal language models. In *Proceedings of the IEEE/CVF Conference on Computer Vision and Pattern Recognition (CVPR)*, pages 21853–21862, 2024. [1](#)
- [72] Yue Zhang, Yafu Li, Leyang Cui, Deng Cai, Lema Liu, Tingchen Fu, Xinting Huang, Enbo Zhao, Yu Zhang, Yulong Chen, Longyue Wang, Anh Tuan Luu, Wei Bi, Freda Shi, and Shuming Shi. Siren’s song in the ai ocean: A survey on hallucination in large language models. *ArXiv*, abs/2309.01219, 2023. [2](#)
- [73] Yao Zhao, Mikhail Khalman, Rishabh Joshi, Shashi Narayan, Mohammad Saleh, and Peter J Liu. Calibrating sequence likelihood improves conditional language generation. In *The Eleventh International Conference on Learning Representations*, 2023. [3](#)
- [74] Lianmin Zheng, Wei-Lin Chiang, Ying Sheng, Siyuan Zhuang, Zhanghao Wu, Yonghao Zhuang, Zi Lin, Zhuohan Li, Dacheng Li, Eric Xing, Hao Zhang, Joseph E Gonzalez, and Ion Stoica. Judging llm-as-a-judge with mt-bench and chatbot arena. In *Advances in Neural Information Processing Systems*, pages 46595–46623. Curran Associates, Inc., 2023. [1](#)
- [75] Bolei Zhou, Agata Lapedriza, Jianxiong Xiao, Antonio Torralba, and Aude Oliva. Learning deep features for scene recognition using places database. In *Advances in Neural Information Processing Systems*. Curran Associates, Inc., 2014. [6](#)
- [76] Chunting Zhou, Graham Neubig, Jiatao Gu, Mona Diab, Francisco Guzmán, Luke Zettlemoyer, and Marjan Ghazvininejad. Detecting hallucinated content in conditional neural sequence generation. In *Findings of the Association for Computational Linguistics: ACL-IJCNLP 2021*, pages 1393–1404, Online, 2021. Association for Computational Linguistics. [2](#)
- [77] Yiyang Zhou, Chenhang Cui, Jaehong Yoon, Linjun Zhang, Zhun Deng, Chelsea Finn, Mohit Bansal, and Huaxiu Yao. Analyzing and mitigating object hallucination in large vision-language models. In *The Twelfth International Conference on Learning Representations*, 2024. [1](#), [2](#), [3](#)

A. Supplementary Experiments and Results

A.1. Experiment Details

Hyperparameter settings In general, we follow the default hyperparameters of each algorithm as proposed by the original authors. Tab. 5 lists the key hyperparameters used in our experiments for both VORD decoding and VORD loss.

Hyperparameters	Values
Learning rate	1e-5
Learning rate scheduler	Cosine
Batch size per GPU	8
Optimizer	Adam
Epochs	1
Temperature (T)	1.0
β	0.2
ψ	1.0 or 2.0
Top P	1.0
Top K	None
Mixup (α)	1.0
No. of bins B	15.0

Table 5. Hyperparameters used in our experiments for VORD.

A.2. VORD Decoding

We detail the individual scores of VORD decoding evaluated on MME (Perception) tasks. Tab. 6 shows the full split of all ten individual perception tasks of MME, evaluated on all three backbone architectures. Our findings show that solely using regular decoding results in the lowest scores, with improvements obtained when using VCD and OPERA, with VORD decoding achieving the highest overall scores.

An interesting observation is that the scores of individual tasks tend to vary across algorithms. For example, on the LLaVA-v-1.5 backbone, we can see that VORD decoding performs best on the Existence task with 185 points, while achieving the lowest score on Position with only 117.22 points. Ideally, we would expect a general improvement across all tasks, leading to the highest overall scores. A possible explanation to this variance in results could be due to the randomness of algorithms used, such as Mixup or Diffusion during image modifications and multinomial sampling during the generation process.

A.3. VORD Loss

We further analyze the improvements of VORD loss evaluated on the POPE and MME benchmarks. Tab. 7 shows the averaged scores of all three datasets of POPE across the random, popular and adversarial settings. We compare the scores of two model backbones LLaVA-v1.5-7B and LLaVA-v1.5-13B, finetuned with and without VORD loss using regular decoding.

Our results consistently demonstrate clear improvements when using VORD loss, with performance gains of roughly +2.5% and +2.0% in model accuracy and F1. While both $\psi = 1$ and $\psi = 2$ yield similar improvements, the squared variant $\psi = 2$ exhibits a slight edge. Based on these findings, we therefore recommend using the squared variant of VORD loss for optimal performance. For completeness, the algorithm of VORD loss for next-word prediction is presented in Algorithm 2.

Algorithm 2: VORD loss

Data: Given training corpus $D_{\text{train}} = (x_i, y_i)_{i=1}^N$

- 1: Initialize LVLM parameters θ
- 2: Begin: $y_0 = \text{BOS}, t = 1$
- 3: **for** $e \in \text{epochs}$ **do**
- 4: $\hat{v} = \alpha * v_1 + (1 - \alpha) * v_2$ // Modify image
- 5: $m_\theta = \frac{1}{\pi} \arccos \left(\frac{\tilde{f}_\theta(v) \cdot \tilde{f}_\theta(\hat{v})}{\|\tilde{f}_\theta(v)\| \|\tilde{f}_\theta(\hat{v})\|} \right)$ // Sim margin
- 6: $P_\theta(y|v, x) = \theta(v, x)$ // Clean image
- 7: $P_\theta(y|\hat{v}, x) = \theta(\hat{v}, x)$ // Modified image
- 8: $\mathcal{L}_{\text{vord}} = \max(P_\theta(y|\hat{v}, x) - P_\theta(y|v, x) + m_\theta, 0)^\psi$
- 9: $\mathcal{L}_{\text{total}} = \mathcal{L}_{\text{CE}} + \mathcal{L}_{\text{VORD}}$
- 10: $\theta_{\text{new}} \leftarrow \theta_{\text{old}} - \eta \nabla_{\theta} \mathcal{L}_{\text{total}}$ // Update parameters θ
- 11: **return** θ

B. Ablation Study

Effects of Different Visual Corruptions While visual corruptions are not the primary focus of our work, for completeness we include these analysis comparing the performances of different noise types. In Tab. 8, we report the performance of VCD and VORD evaluated on different visual corruptions.

Specifically, we compare eleven corruption types including Mixup, Diffusion noise and nine other common image corruptions [17]. Our findings demonstrate that VORD delivers the best performance gains on most corruptions types, with the greatest improvements in F1 obtained from Mixup and Diffusion. To gain further insights, we analyzed the averaged similarity margins m_θ between original and perturbed images for each corruption type. We observed that less significant corruptions, leading to smaller margins, limit the activation of VORD’s transitive property, thereby reducing its effectiveness. For instance, corruptions such as “Jpeg Compression”, “Gaussian Blur”, “Brightness” and “Saturate” which typically result in smaller margins $m_\theta \leq 0.034$, yielded relatively lower performance compared to VCD.

Conversely, more significant corruptions such as “Mixup” and “Diffusion” with larger margins *e.g.* $m_\theta \geq 0.081$, enabled VORD to fully utilize its transitive property and achieve the best performance. This suggests that corruptions used to generate the modified image have to be significant, in order to better enable to contrasting between the probability distributions of the original and modified images. This experiment highlights the following three key findings:

- **VORD contrasts better than VCD:** Despite the varying effects of different visual corruption types, VORD outperforms VCD on most corruption types.
- **Visual corruptions have to be significant:** For the optimal performance of VORD, the visual corruptions applied on the modified image has to be “severe” enough for a large enough margin and visual contrasting to occur.
- **The Synergy of VORD and Mixup:** The combination of VORD and Mixup yields the most significant improvements in F1, suggesting that VORD effectively leverages the benefits of Mixup to enhance its performance.

Model	Method	MME Tasks (Perception)										Overall Scores \uparrow
		Existence	Count	Position	Color	Posters	Celebrity	Scene	Landmark	Artwork	OCR	
LLaVA-v1.5	Regular	181.67 \pm 2.36	111.67 \pm 19.77	118.89 \pm 1.57	140.56 \pm 6.98	124.60 \pm 3.36	112.65 \pm 1.44	147.58 \pm 3.91	131.25 \pm 3.89	108.50 \pm 4.64	117.50 \pm 10.8	1294.86 \pm 21.20
	VCD	181.67 \pm 2.36	122.78 \pm 13.63	121.67 \pm 1.36	143.89 \pm 6.29	126.98 \pm 3.85	134.71 \pm 2.60	155.58 \pm 1.65	141.58 \pm 0.51	112.42 \pm 2.26	115.00 \pm 3.54	1356.27 \pm 20.05
	OPERA	180.67 \pm 0.00	133.33 \pm 0.00	123.33 \pm 0.00	155.00 \pm 0.00	134.69 \pm 0.00	116.76 \pm 0.00	152.75 \pm 0.00	133.01 \pm 0.00	103.25 \pm 0.00	100.00 \pm 0.00	1332.79 \pm 0.00
	VORD (Ours)	185.00 \pm 4.08	132.22 \pm 11.57	117.22 \pm 3.42	145.56 \pm 9.06	133.45 \pm 3.93	141.47 \pm 3.39	154.17 \pm 1.03	151.67 \pm 1.01	117.17 \pm 4.85	115.83 \pm 6.29	1393.75 \pm 20.29
Qwen-VL	Regular	145.00 \pm 15.0	115.83 \pm 2.50	122.5 \pm 5.83	176.67 \pm 1.67	136.73 \pm 6.46	121.76 \pm 0.29	148.62 \pm 1.62	159.12 \pm 2.62	125.00 \pm 2.00	101.25 \pm 1.25	1352.49 \pm 21.31
	VCD	156.00 \pm 6.52	131.00 \pm 6.19	128.00 \pm 3.61	181.67 \pm 5.14	142.45 \pm 2.96	137.35 \pm 2.45	149.10 \pm 2.51	163.95 \pm 1.77	127.65 \pm 2.81	86.00 \pm 3.35	1403.17 \pm 14.57
	OPERA	165.00 \pm 0.00	118.33 \pm 0.00	138.33 \pm 0.00	180.00 \pm 0.00	142.18 \pm 0.00	118.53 \pm 0.00	157.00 \pm 0.00	160.75 \pm 0.00	132.75 \pm 0.00	87.50 \pm 0.00	1400.37 \pm 0.00
	VORD (Ours)	165.00 \pm 0.10	120.56 \pm 5.67	128.33 \pm 8.16	181.67 \pm 2.36	143.65 \pm 3.53	129.71 \pm 2.53	154.42 \pm 1.53	166.17 \pm 3.16	135.08 \pm 3.14	102.50 \pm 6.12	1427.07 \pm 22.90
InstructBLIP	Regular	153.33 \pm 0.10	80.00 \pm 0.10	65.00 \pm 0.10	108.33 \pm 0.10	98.98 \pm 0.10	97.35 \pm 2.16	130.50 \pm 0.10	103.25 \pm 0.10	85.25 \pm 5.59	55.00 \pm 0.10	976.99 \pm 27.70
	VCD	162.78 \pm 6.98	90.00 \pm 4.08	65.56 \pm 4.16	118.89 \pm 10.30	109.30 \pm 2.80	120.78 \pm 3.96	134.33 \pm 2.70	125.83 \pm 3.68	92.17 \pm 4.12	69.17 \pm 11.61	1088.80 \pm 28.58
	OPERA	175.00 \pm 0.00	55.00 \pm 0.00	50.00 \pm 0.00	118.15 \pm 0.00	122.86 \pm 0.00	80.00 \pm 0.00	149.25 \pm 0.00	138.79 \pm 0.00	90.75 \pm 0.00	65.00 \pm 0.00	1044.80 \pm 0.00
	VORD (Ours)	164.44 \pm 4.78	85.00 \pm 1.36	65.00 \pm 1.36	134.44 \pm 3.42	113.95 \pm 5.42	119.31 \pm 2.93	138.67 \pm 5.42	132.75 \pm 5.62	96.08 \pm 2.97	83.33 \pm 4.25	1132.98 \pm 29.06

Table 6. Detailed results (%) comparing different decoding methods computed across 3 seeds, evaluated on the perception subset of MME.

Datasets	Setting	Model	Method	Accuracy \uparrow	Precision \uparrow	Recall \uparrow	F1 \uparrow	ECE \downarrow
(Avg. scores of) MSCOCO + GQA + A-OKVQA	Random	LLaVA-v1.5-7B	Baseline	83.90 \pm 0.29	89.24 \pm 0.41	77.64 \pm 0.36	82.96 \pm 0.30	2.82 \pm 0.11
			VORD loss ($\psi = 1$)	86.46 \pm 0.12	91.62 \pm 0.27	80.81 \pm 0.20	85.74 \pm 0.12	2.94 \pm 0.15
			VORD loss ($\psi = 2$)	85.80 \pm 0.19	92.41 \pm 0.36	78.54 \pm 0.17	84.78 \pm 0.18	3.01 \pm 0.12
		LLaVA-v1.5-13B	Baseline	84.20 \pm 0.23	89.08 \pm 0.46	78.46 \pm 0.28	83.36 \pm 0.22	2.65 \pm 0.08
			VORD loss ($\psi = 1$)	85.83 \pm 0.26	91.63 \pm 0.29	79.41 \pm 0.49	84.95 \pm 0.30	2.74 \pm 0.08
			VORD loss ($\psi = 2$)	85.85 \pm 0.12	92.05 \pm 0.13	79.00 \pm 0.36	85.03 \pm 0.15	3.04 \pm 0.08
	Popular	LLaVA-v1.5-7B	Baseline	80.27 \pm 0.52	82.50 \pm 0.56	77.45 \pm 0.56	79.72 \pm 0.54	3.14 \pm 0.04
			VORD loss ($\psi = 1$)	82.06 \pm 0.24	83.82 \pm 0.25	80.4 \pm 0.27	81.79 \pm 0.26	3.31 \pm 0.06
			VORD loss ($\psi = 2$)	82.78 \pm 0.32	86.38 \pm 0.43	78.47 \pm 0.24	81.99 \pm 0.31	3.56 \pm 0.06
		LLaVA-v1.5-13B	Baseline	81.83 \pm 0.40	84.48 \pm 0.60	78.34 \pm 0.41	81.16 \pm 0.39	2.85 \pm 0.08
			VORD loss ($\psi = 1$)	81.53 \pm 0.12	83.93 \pm 0.17	78.91 \pm 0.07	81.07 \pm 0.10	2.96 \pm 0.08
			VORD loss ($\psi = 2$)	82.05 \pm 0.12	84.65 \pm 0.13	79.12 \pm 0.36	81.79 \pm 0.15	2.94 \pm 0.08
Adversarial	LLaVA-v1.5-7B	Baseline	76.39 \pm 0.38	76.36 \pm 0.34	77.42 \pm 0.55	76.68 \pm 0.40	5.63 \pm 0.09	
		VORD loss ($\psi = 1$)	78.22 \pm 0.21	77.91 \pm 0.18	80.35 \pm 0.19	78.75 \pm 0.18	5.82 \pm 0.10	
		VORD loss ($\psi = 2$)	78.73 \pm 0.15	79.83 \pm 0.21	78.04 \pm 0.02	78.62 \pm 0.12	5.85 \pm 0.07	
	LLaVA-v1.5-13B	Baseline	78.11 \pm 0.22	78.44 \pm 0.27	78.25 \pm 0.21	78.17 \pm 0.20	5.11 \pm 0.06	
		VORD loss ($\psi = 1$)	78.09 \pm 0.15	78.27 \pm 0.17	79.19 \pm 0.37	78.40 \pm 0.16	5.74 \pm 0.08	
		VORD loss ($\psi = 2$)	78.25 \pm 0.12	78.50 \pm 0.13	78.66 \pm 0.36	78.55 \pm 0.15	5.82 \pm 0.08	

Table 7. We report the averaged results (%) of VORD loss evaluated on all three datasets of the POPE benchmark.

Model	Method	POPE MSCOCO (F1 \uparrow)										
		Mixup	Diffusion	Jpeg Compression	Gaussian Noise	Shot Noise	Impulse Noise	Speckle Noise	Gaussian Blur	Contrast	Brightness	Saturate
LLaVA-v1.5	VCD	83.05 \pm 0.09	82.54 \pm 0.21	82.25 \pm 0.13	82.34 \pm 0.29	82.16 \pm 0.14	82.32 \pm 0.19	82.23 \pm 0.18	82.18 \pm 0.12	82.28 \pm 0.24	82.37 \pm 0.12	82.11 \pm 0.14
	VORD (Ours)	84.21 \pm 0.19	83.63 \pm 0.21	81.99 \pm 0.14	83.07 \pm 0.30	82.70 \pm 0.41	83.16 \pm 0.29	82.87 \pm 0.46	80.83 \pm 0.20	82.74 \pm 0.18	81.97 \pm 0.16	81.46 \pm 0.27
	Similarity Margin	0.131	0.081	0.030	0.056	0.049	0.059	0.055	0.030	0.054	0.034	0.027

Table 8. Ablation study for different corruption/noise types evaluated on POPE. Strong visual corruptions, such as Mixup, are recommended in order to maximize VORD’s performance gains.

C. Case Studies

C.1. GPT4o-Aided Evaluation on LLaVA-Bench

This section describes the process of evaluating output text responses on GPT4o. As mentioned in our main paper, we prompt each backbone LLM with “Describe this image in detail.” conditioned upon the images provided in LLaVA bench. The total word count of each response are collected and averaged over three runs and reported in Tab. 3.

Prompt Card for GPT4o All responses and images are collected and evaluated on GPT4o, with an example of the prompt card used provided in Fig. 7. Following which, GPT4o provides a two numerical scores for the accuracy and detailedness of each response. These scores are then averaged across questions and presented in Tab. 3.

Description:

AI that scores image description accuracy and detailedness.

Instructions:

You are an AI designed to evaluate and score the performance of two AI assistants in describing a given image. Your primary focus is on the accuracy and detailedness of their descriptions. You will assess the accuracy by checking for hallucinations - any part of the description that is inconsistent with the image content. For detailedness, you will consider how rich the response is in necessary details, excluding any hallucinated parts. You will provide scores on a scale from 1 to 10 for each assistant separately, based on these criteria. After scoring, you will offer an explanation for your evaluation, ensuring it is free from bias and not influenced by the order of presentation of the responses

Input format:

[Start of Assistant 1]
{Response 1}
[End of Assistant 1]

[Start of Assistant 2]
{Response 2}
[End of Assistant 2]

Output format:

Accuracy:
Scores of the two answers:
Reason:
Detailedness:
Scores of the two answers:
Reason:

Figure 7. Example of prompt-card used on GPT4o, evaluating the accuracy and detailedness of responses.